Aquacultural Engineering 98 (2022) 102263

Contents lists available at ScienceDirect

Aquacultural Engineering

journal homepage: www.elsevier.com/locate/aque

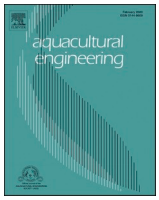

Ultrasonic monitoring of early larval development of fish in tanks. Case study: Gilthead seabream (*Sparus aurata*)

A. Ladino [a,*], V. Puig-Pons [a], V. Espinosa [a], I. Pérez-Arjona [a], F. de la Gándara [b], A. Ortega [b]

[a] Institut d'Investigació per a la Gestió Integrada de Zones Costaneres (IGIC), Universitat Politècnica de València (UPV), Camí de Vera (s/n), 46022 València, Spain
[b] Instituto Español de Oceanografía (IEO), C/Varadero, 1, 30740 San Pedro del Pinatar, Murcia, Spain

ARTICLE INFO

Keywords:
Sparus aurata larvae
Target strength
Swimbladder, aquaculture
Numerical simulation

ABSTRACT

Swimbladder inflation is a significant matter in intensive fish farming, since it is related to larval survival rate and the morphological quality of individuals. In this work, we propose a non-invasive acoustic technique using ultrasound to monitor the swimbladder development of gilthead seabream (*Sparus aurata*) in tanks. The fundamental hypothesis is that, due to the high acoustic contrast of gas, the swimbladder's inflation process can be detected by measuring the larvae's target strength during their early development. Backscatter numerical models using the finite element method, developed from biological measurement data, were applied to evaluate the feasibility of the proposed method. The acoustic measurements were obtained using an EK60 Simrad echosounder working at 200 kHz. The target strength values were evidenced with and without the presence of a developed swimbladder, showing a statistically significant relationship with the swimbladder's standard length, area and the percentage of larvae with a swimbladder. The experiments were carried out in the Spanish Institute of Oceanography (IEO)'s marine aquaculture plant at Mazarrón (Murcia, Spain).

1. Introduction

Gilthead seabream (*Sparus aurata*) is the main species in Mediterranean aquaculture by volume of production, with total production in Europe and the rest of the Mediterranean in 2020 coming to 278,199 tonnes (APROMAR, 2021). The larvae are generally produced in tanks and the fingerlings are transferred to floating sea cages to complete the rearing process.

Optimal rearing conditions for gilthead seabream larvae include swimbladder inflation during their early period of development, which is expected to occur when the larvae's length reaches around 4 mm, and the maximum inflation rate is supposed to be found around 15 days post-hatch (Chatain and Ounais-Guschemann, 1990; Chatain, 1986).

Non-inflation of the swim bladder in marine fish is a major problem for larval rearing, leading to an increase in larval mortality at an early stage (Modica et al., 1993; Woolley and Qin, 2010). The absence of a swimbladder has been associated with significant physiological problems, some of the most significant of which are spinal deformities and lordosis (Andrades et al., 1996; Chatain, 1994). Gilthead seabream rearing studies have shown the consequences of an uninflated swimbladder,finding abnormal morphoanatomical deficiencies in the osteological development and skeletal anomalies (Boglione et al., 2001; Prestinicola et al., 2014). Moreover, the growth rate of larvae without a functional swimbladder could be reduced because of greater energy expenditure to maintain their swimming position in the water column, since the swimbladder enables buoyancy control. For this reason, non-activation of the swimbladder in the early stages of development leads to an increase in larval mortality rate in the aquaculture industry (Moretti et al., 1999).

Ultrasonic techniques have proven to be an effective method to monitor the abundance of fish stocks and to estimate biomass in a non-intrusive way (Li et al., 2020), thereby respecting current legislation on animal welfare. To do so, target strength (TS) is used (Simmonds and MacLennan, 2005), which is defined as the ratio between backscattered and incident acoustic intensities when a target is insonified. The target strength depends on many factors, including acoustic frequency, absence or presence of a swimbladder, fish size and behaviour, as well as fish morphology and their swimming tilt with respect to the acoustic transducer (Foote, 1987; Furusawa, 1988). Many species of fish, including gilthead seabream, possess a gas-filled swimbladder. This gas has a high acoustic contrast, which means the swimbladder acts as a great reflector of acoustic energy. Hence, when there is a swimbladder

* Corresponding author.
E-mail addresses: anlave@doctor.upv.es (A. Ladino), vipuipon@upv.es (V. Puig-Pons), vespinos@upv.es (V. Espinosa), iparjona@upv.es (I. Pérez-Arjona), fernando.delagandara@ieo.es, anlave@upv.es (F. de la Gándara), aurelio.ortega@ieo.es (A. Ortega).

https://doi.org/10.1016/j.aquaeng.2022.102263
Received 12 January 2022; Received in revised form 5 May 2022; Accepted 6 May 2022
Available online 11 May 2022

present, it is responsible for 90–95% of the total backscattered acoustic energy from the fish (Foote, 1980; Ona, 1990). Following this assumption, this work proposes to detect the swimbladder's inflation during the larval evolution process by using ultrasonic acoustic techniques.

The relationship between TS and length (L) for different fish species has been studied widely (Love, 1971; Simmonds and MacLennan, 2005), but few investigations on this relationship for larvae have appeared. However, a regression between Atlantic cod larvae (*Gadus morhua*) length and TS has been studied (Chu et al., 2003) using 350–650 kHz broadband transducers. Other studies estimate the TS vs L relationship for Japanese anchovy larvae (*Engraulius japonicus*) using the theoretical scattering model to calculate TS at 120 kHz (Ito et al., 2011). In addition, scattered acoustic energy has been used to estimate larval abundance (*Chaoborus flavicans*) and to monitor larvae diel migration using a multifrequency system (Knudsen et al., 2006; Knudsen and Larsson, 2009).

This paper, however, uses a method to monitor gilthead seabream (*Sparus aurata*) swimbladder inflation and early larval development in offshore tanks. The main hypothesis is that, due to the high acoustic contrast of gas, the acoustic backscattered energy increases significantly when swimbladder inflation occurs, so swimbladder development and larval growth can be monitored using echosounding techniques. To evaluate the feasibility of this premise, a numerical simulation of seabream larvae target strength was developed using the finite element method. To validate the numerical results, ventral TS measurements were obtained using a scientific Simrad EK60 echosounder. The acoustic measurements were initially analysed in the absence of an aeration system to avoid the presence of air bubbles that could be confused with gas-filled swimbladders, thus ensuring the proposed method's detection capability. In order to confirm the validity of the method under production conditions, TS measurements were also taken with an aeration system working. From these measurements, the TS vs larvae length relationship was established. In addition, the detection of inflated swimbladder presence using ultrasound was investigated and the relationship between TS vs percentage of swimbladder inflation was shown.

2. Materials and methods

Data were collected in two consecutive experiments, referred to as Experiment 1 (Exp1) and Experiment 2 (Exp2), performed in May and June in the Spanish Oceanographical Institute (IEO)'s marine aquaculture plant in Puerto de Mazarrón (Murcia, Spain). Approximately 300,000 gilthead seabream (*Sparus aurata*, Linnaeus, 1758) eggs were inoculated in each experiment in the larval rearing units (20 m^3 indoor tanks with a diameter of 4 m and depth of 1.7 m). Aeration and a flow-through system was used. Sea water was UV-filtered at a daily exchange rate of 50–100%, and the temperature was maintained almost constant, oscillating between 19.1 and 21.0 °C (Exp1) and between 19.6 and 22.4 °C (Exp2). Larvae were fed as of 2-dph with Brachionus plicatilis rotifers. Once a day, the rotifer concentration was counted and then topped up to ensure 10 rotifer/ml. In order to keep up an adequate nutritional quality with the rotifers, Nannochloropsis gaditana or DHA-enriched *Chlorella* (Pacific Trade Aquaculture Ltd) were added daily to the larval rearing tanks. The tank had a surface cleaning system (skimmer) to keep the surface free from lipids and to ensure the larvae's swimbladder inflation (Georgakopoulou et al., 2010; Kurata et al., 2012). The gilthead seabream larvae's photoperiod was 12 h (light between 8:00 a.m. and 8:00 p.m.; and 12 h of darkness). As the tanks were placed in an indoor facility, an artificial lighting system was used. The larvae were acoustically monitored from day 4 post-hatch (4-dph) to day 16 post-hatch (16-dph), and direct biological measurements were continued up to 17-dph in both experiments.

2.1. Biological and environmental data acquisition

In order to obtain direct information about the larvae's growth and swimbladder inflation, representative samples of 25–50 larvae were taken daily. According to previous studies (Brewer and Kleppel, 1986; Davis et al., 1990; Del Pilar Ruso and Bayle-Sempere, 2006; Leis, 2004; Murphy et al., 2011; Neilson and Perry, 1990; Shoji et al., 1999), from the moment of hatching, vertical migration is the usual pattern of behaviour in larvae, with nocturnal ascent the most observed swimming pattern for marine fish larvae. Such vertical migrations are more frequent after swimbladder inflation due to the enhanced swimming capacity. To improve the monitoring of swimbladder inflation, the larvae were sampled at night, since that is when the swimbladders swell to help the larvae's ascent in the water column in the dark period, so it is the most suitable time to measure them (Woolley and Qin, 2010; Kitajima et al., 1985).

The larvae's size was measured using a Leica MS5 optical microscope with a Leica S3 high-definition camera. To process the recorded images, Leica Application Suite (LAS 123) software was used. The standard length and swimbladder area (when the swimbladder was present) were measured. Standard length (L_s) refers to the measurement from the tip of the snout to the end of the notochord (Fig. 6b). The survival rate was estimated by counting the larvae in a certain volume (increasing from 10 to 50 l throughout the experiment). The swimbladder area (∅) is defined as the maximum area of a plane perpendicular to the z-axis (Fig. 6b). The recorded images provided a repository that allowed the larvae's geometry to be modelled and used in the numerical TS estimation, in the analysis of TS measurements and in their relationship with larval development.

Abiotic parameters were also monitored daily: the temperature was measured using a high-precision digital thermometer (Hanna Instruments Checktemp 1); salinity was recorded with an optical hand refractometer (Atago S-10E); standing at around 37.5 ppt; and dissolved oxygen was measured with a Handy Polaris sensor, remaining close to 100% saturation. Temperature and salinity were used as input parameters for the acoustic data processing.

2.2. Acoustic scattering model of gilthead seabream larvae

To evaluate the feasibility of monitoring the gilthead seabream larvae's growth and swim-bladder development, a model for acoustic scattering for seabream larvae was developed, where the body and swimbladder shapes were obtained from the image repository generated from the biological sampling. A numerical model using the finite element method (FEM) was implemented (Ihlenburg, 1998; Jech et al., 2015; Langdon, 2007). In this case, FEM solves the inhomogeneous Helmholtz equation in three dimensions for the scattered pressure field from an incident plane wave defined in the larvae's internal bodies:

$$\nabla \bullet \left(\frac{-\nabla p}{\rho}\right) - \frac{w^2}{\rho c^2} p = 0 \tag{1}$$

where p is the acoustic pressure $[Pa]$, ρ is the density $[kgm^{-3}]$, w is the angular frequency $[2\pi f, rads^{-1}]$ and c the speed of sound $[ms^{-1}]$. The study was carried out in a harmonic regime with the acoustic module in the frequency domain:

$$p(\bar{r}, t) = p(\bar{r}) e^{iwt} \tag{2}$$

where $\bar{r}$ is the position vector $[m]$ and t the time $[s]$. In the numerical model, sound speed and density vary with space, while the pressure varies with space and implicitly with time.

The simulation was developed considering the real geometry of the gilthead seabream larvae (Ceballos-Francisco et al., 2020), using two-dimensional images taken in the experiments as reference (Fig. 6). The 3D models were constructed taking into account the acoustic contribution from the main internal structures (Pérez-Arjona et al., 2020): the fin, notochord, oil globule and swimbladder (when developed). Initially, the swimbladder is spherical in shape, becoming longer and elongated over the subsequent days in this early development stage.

In our model, the swim bladder was modelled as a prolate spheroid (Chu et al., 2003) whose dimensions were chosen from the microscope images. It is known that TS is defined as $TS = 10\log(\sigma_{bs})$, where σ_{bs} is the backscattering cross-section of an individual. The backscattering cross-section is related to the ventral cross-section of the target (Simmonds and MacLennan, 2005). Following this assumption, to model the swimbladder we defined a prolate spheroid with the longitudinal length and transversal cross-section as observed in the biological samples.

In the absence of exact values for the material properties of the gilthead seabream larvae's internal tissues, reference values for sound velocity, c, and volumetric density, ρ, were used: c_{fin}= 1537 m/s and ρ_{fin}= 1060 kg/m^3 for the body fin, c_{not}= 2600 m/s and ρ_{not}= 1130 kg/m^3 for the notochord (Boyra et al., 2018; Gorska et al., 2007), and c_{oil}= 1450 m/s and ρ_{oil}= 920 kg/m^{3}for the oil globule (Tsaklis, 2010). Scattering objects were considered to be fluid-like, while pressure release boundary condition was applied on the boundary of the swimbladder (c_{air}=343 m/s, ρ_{air}=1.21 kg/m^3), allowing a computational saving (Jech et al., 2015). The surrounding medium is considered to be water (c_w=1490 m/s, ρ_w=1030 kg/m^3) with an artificial absorption layer to avoid PML (Perfectly Matched Layers) and computational reflections (Berenger, 1996; Zampolli et al., 2007).

The incident acoustic wave was considered to be a plane wave along the positive y-axis direction, impinging on the ventral part of the larvae, at an ultrasonic working frequency of 200 kHz (Fig. 1). To guarantee the proper density mesh, the meshing domain was developed by free and adjusted tetrahedral finite elements for each component with a mesh size of λ/10 (Ihlenburg, 1998). The far-field backscattered acoustic pressure field was estimated by evaluating the Helmholtz-Kirchhoff integral on the boundary between the surrounding medium and PML (Comsol, 2021; O'Driscoll et al., 2011; Pierce, 2019).

2.3. Acoustic data acquisition

A 200 kHz split-beam transducer (ES200-7C) operated by a Simrad EK60 echosounder was used with a transmitting power of 45 W, a pulse length of 64 μs and 1 ping per second. The transducer (ES200-7C) had a nominal angle of 7° (Table 1). The on-axis and off-axis calibration was carried out using the standard calibration method, with a 13 mm diameter copper sphere to calibrate the 200 kHz echosounder (Simrad, 2008).

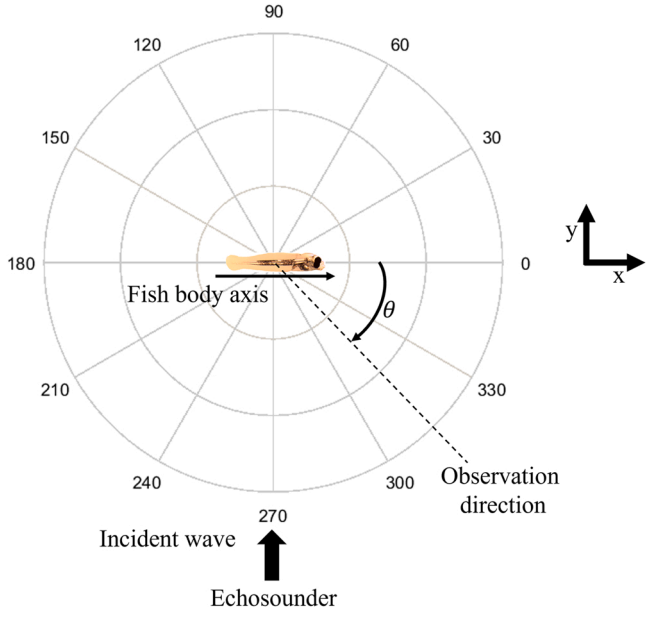

Fig. 1. Diagram of the directivity $D(\theta)$ calculation in the x-y plane, where θ is the observation angle; $\theta = 0°$ is the direction of the fish's head, $\theta = 180°$ is the direction of the fish's tail, and $\theta = 270°$ is the direction of the center of the echosounder's transducer.

Table 1
Parameters of acoustic systems (Simrad EK60) and filtering parameters used to detect single targets.

	200 kHz
Ping interval (s^{-1})	1
Transducer gain (dB)	24.48
Transmitted pulse duration (ms)	0.064
Power (W)	45
Two-way beam angle (dB)	-20.7
Minor axis3dB beam angle (°)	6.35
Major axis 3 dB beam angle (°)	6.41
Minimum TS threshold (dB)	-90
Minimum echolength ratio with pulse duration	0.4
Maximum echolength ratio with pulse duration	4
Maximum phase deviation	0.5
Maximum gain compensation (dB)	3

The transducer was looking on a platform recording the ventral view of the larvae and placed at the bottom of the tank (1.3 m deep). To avoid aeration systems, the equipment was located in the middle of the tank's radius (Fig. 2).

2.4. Acoustic data measurement processing

Two different operating conditions were considered in the acoustic measurements: control and production conditions. The control conditions were defined as the aeration system being switched off. Production conditions were the normal rearing conditions in tanks, with the aeration and flow-through systems working.

Acoustic data were analysed using our own software developed in Matlab®. Fig. 3 shows the sequence of acoustic data processing automatic algorithm. Compensated target strength (TS) was calculated in a thin layer between 0.4 and 1.2 m form the tank's bottom. In this region, the larvae's distance to the acoustic transducer was further than the critical range (Rc) or Fresnel distance. In the case of the Simrad ES200-7C transducer's characteristics, the critical range is at 0.33 m. At working distances larger than Rc, the directivity pattern of the ultrasonic beam is stable and the field amplitude decreases monotonically. Nevertheless, the acoustic field does not show spherical spreading until it propagates 2–4 times the Fresnel distance (Rc) (Simmonds and MacLennan, 2005). According to previous studies, measurements conducted in a range between Rc and 4Rc can be corrected to compensate for amplitude decay (Sobradillo et al., 2021). TS values were corrected using the theoretical range-dependence of the pressure wave of a circular piston, simulating the geometry of a Simrad ES200-7C transducer (Sobradillo et al., 2021). Applying such a correction allows the working distance to be increased and as well as the number of quality acoustic detections. This is relevant in the case of arrangements with short working distances like cages or, as in this case, tanks. Once the TS correction was applied, the median of the compensated TS values was obtained. The acoustic measurements were continuously performed from 6-dph to the end of the experiment.

In order to obtain the median TS, a Single Echo Detection (SED) algorithm was applied to reduce the larvae echo to a single linear track. The SED parameters used are shown in Table 1. As usual, a minimum TS threshold (−90 dB) was set to apply SED, and in this case a maximum TS threshold (−50 dB) was also used to eliminate the contribution from big bubbles from aeration systems.

To validate the main hypothesis and confirm that larvae can be detected and monitored by acoustic techniques, a manual detection of individual larvae traces was implemented for the measurements in Experiment 1. An experienced operator identified the traces under the following additional restrictions: not following an ascending path in the tank (to avoid confusion with air bubbles) and satisfying a minimum trace length (at least 3 pings). Once the working hypothesis was

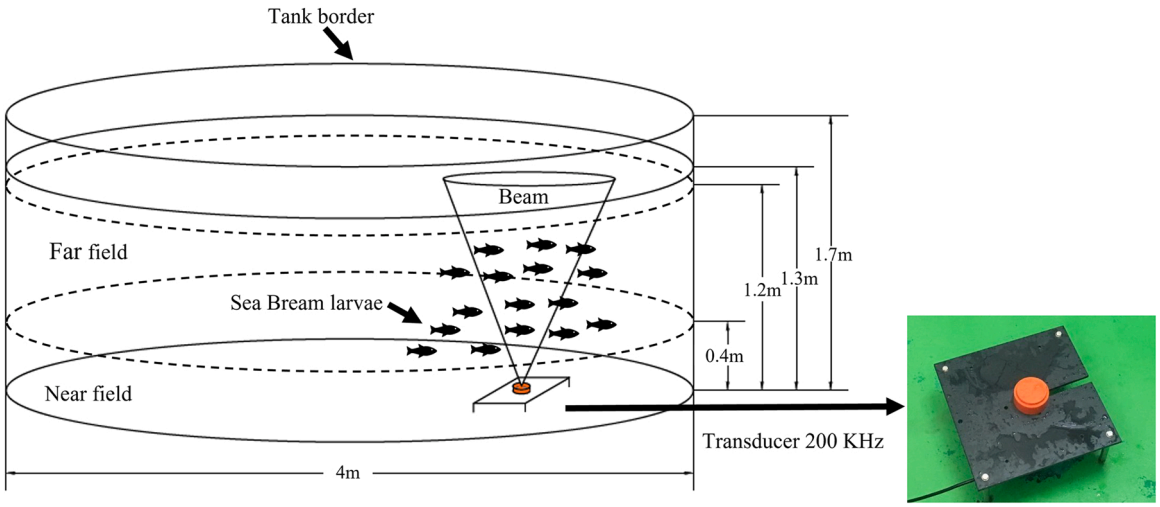

Fig. 2. Experimental setup. Setup diagram (left panel): 200 kHz transducer mounted on a platform at the bottom of the tank facing the surface. (Right panel): transducer and platform used in the experiments.

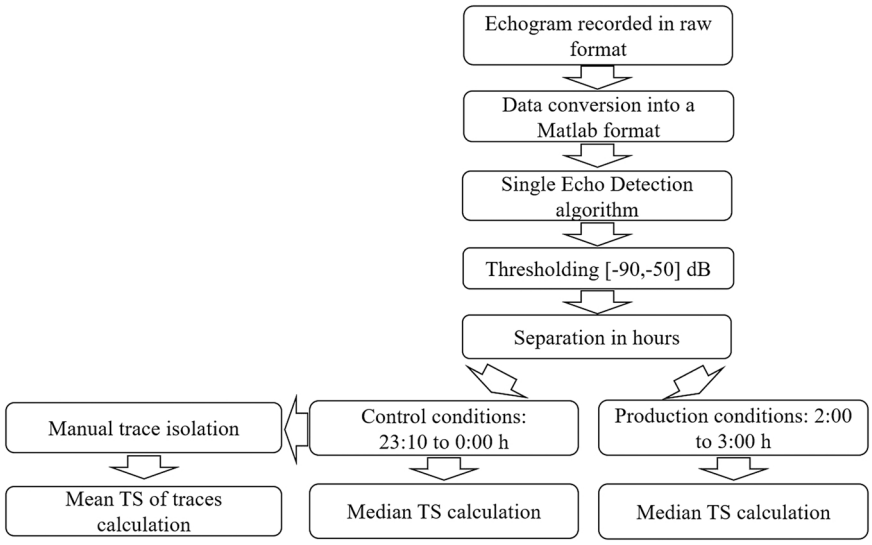

Fig. 3. The sequence of acoustic data processing automatic algorithm in Matlab.

confirmed, an algorithm of our own was implemented in Matlab® to automate the processing of the acoustic data obtained after applying the SED algorithm.

Control data were analysed separately from data recorded under production conditions (Fig. 4). The aeration system was switched off daily from 23:00–00:00 h. In order to avoid residual bubbles from the aeration system after switching off, the first ten minutes from the control records were removed from the calculation of the median TS. Hence, the median TS under control conditions was calculated every day with measurements obtained from 23:10–00:00 h.

The median TS corresponding to production conditions was calculated every day for one hour from 02:00–03:00 h.

3. Results

3.1. Results from biological sampling

Fig. 5 shows the evolution of the standard length (L_s) and the area of the swimbladder's maximum cross-section (∅) for the larvae over time. According to Georgakopoulou et al. (2010), Vizcaíno et al. (2016), the growth of seabream larvae is slow until 60 days compared to their body weight. In all experiments, from 4-dph to 7-dph it was seen that variation of the standard length is small: from 3.75±0.19 mm to 3.85±0.1 mm (Exp1) and from 3.78±0.14 mm to 4.0±0.3 mm (Exp2). The first inflation of the swimbladder was detected in individuals at 7-dph (Exp1) or 8-dph (Exp2), corresponding to an average length L_s = 3.85 mm (Exp1) and L_s = 4 mm (Exp2), in good agreement with previous studies (Chatain, 1986; Chatain and Ounais-Guschemann, 1990). From that moment, larval size increases more rapidly (Fig. 5), associated with better development of mobility after the inflation of the swimbladder. Similar behaviour has been reported in previous studies in reared red seabream larvae (*Pagrus major*) (Kitajima, 1981). The average growth rate after the first inflation detection was 0.203 mm per day (Exp1) and 0.205 mm per day (Exp2), whereas the average growth rate from 4-dph to the initial inflation day was 0.01 (Exp1) and 0.062 (Exp2). The swimbladder's cross-sectional area increased from ∅ = 0.004±0.002 mm^2 to ∅ = 0.09± 0.02 mm^2 (Exp1) and from ∅ = 0.016±0.003 mm^2 to ∅ = 0.10±0.03 mm^2 (Exp2). Fig. 4 also shows the relationship between the swimbladder's cross-sectional area and the standard length of the larvae. The evolution of L_s and ∅ with dph was analysed through linear regression models, obtaining good correlation coefficients in both cases (Table 2). The relationship between ∅ and L_s was also explored,

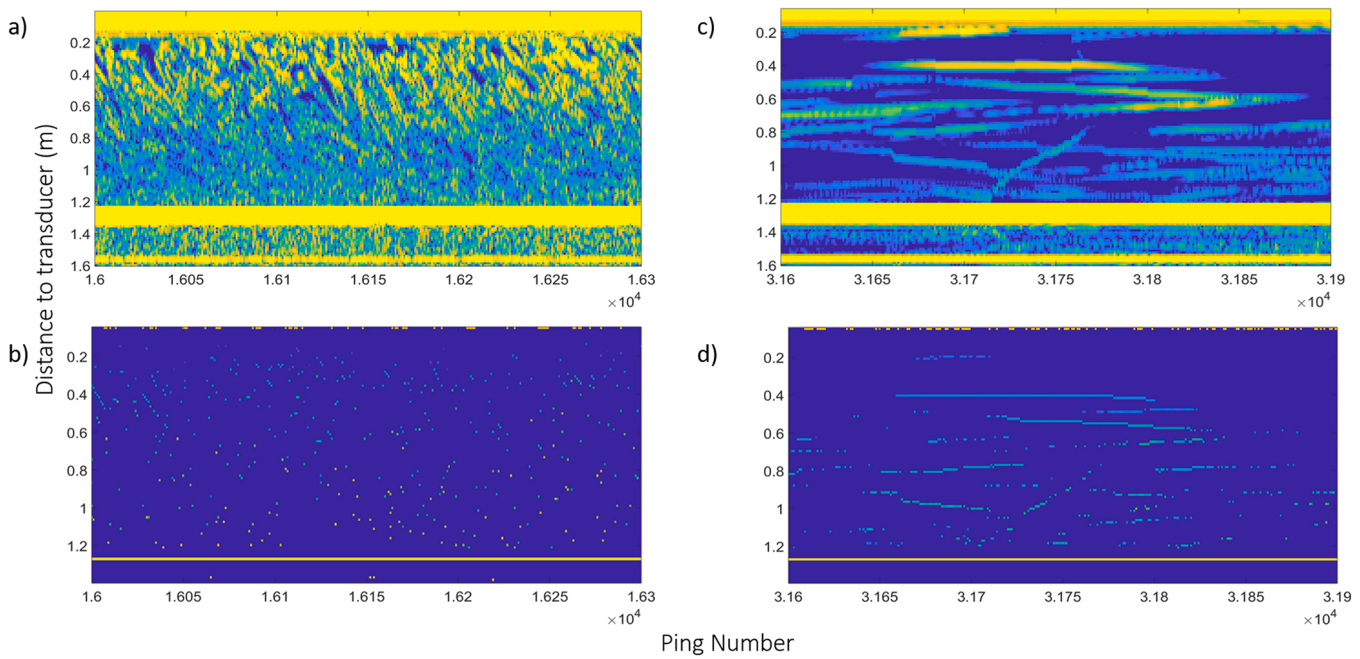

Fig. 4. (a) Echogram obtained in the tank under production conditions. (b) Echogram obtained under control conditions. (c) SED echogram under production conditions. (d) SED echogram under control conditions.

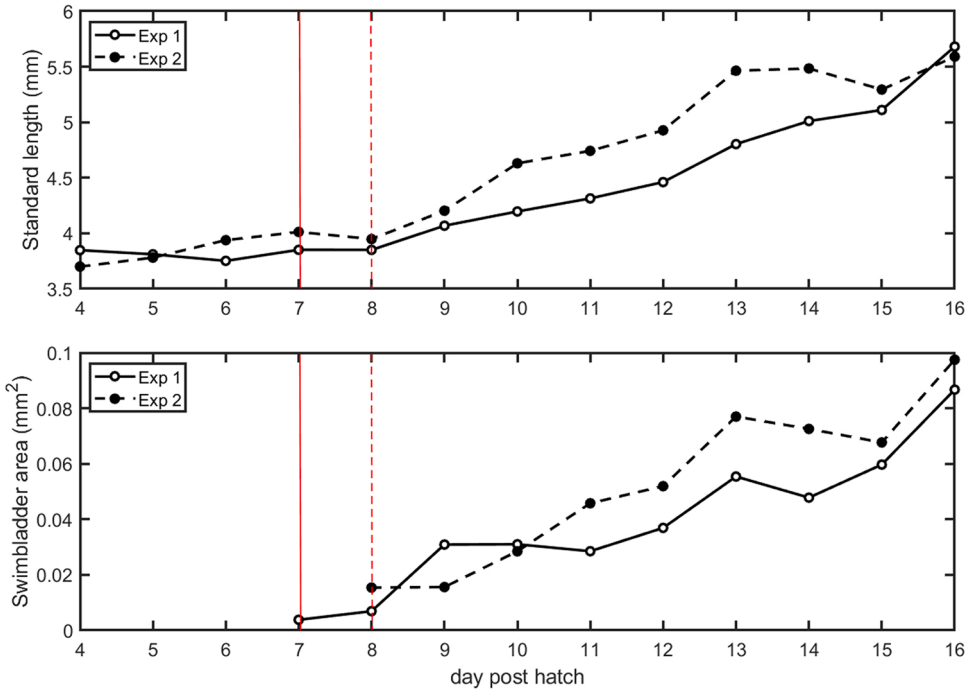

Fig. 5. Value of the median standard length (L_s)– upper panel- and swimbladder area (∅) –lower panel- versus day post-hatch for Exp 1 (solid line) and Exp 2 (dashed line). Vertical solid (Exp 1) and dotted (Exp 2) lines indicate the first detection of inflated swimbladders.

Table 2
Summary of the parameters from the linear regression of the relationship between *Ls* and ∅ for Exp 1 and Exp 2.

	$\varnothing(mm^2) = a \bullet Ls(mm) + b$				
Experiment	a	b	r	r^2	p
Exp1	0.04	-0.14	0.97	0.93	< 0.01
Exp2	0.05	-0.18	0.96	0.91	< 0.01

giving rise to a good correlation of linear regression fit, to be further used to develop the numerical model (Table 2).

Fig. 6 shows the percentage of larvae with an inflated swimbladder (% SBI) during early development. The initial inflation of the swimbladder was detected for the first time between 7-dph and 8-dph, with 2% of the larvae in Exp1 (L_s=3.85±0.24 mm) and 5% of the larvae in Exp2 (L_s=3.9±0.3 mm). Considering that the maximum inflation rate is reached around 15-dph and no further change is expected later (Chatain and Ounais-Guschemann, 1990), measurements were taken up to

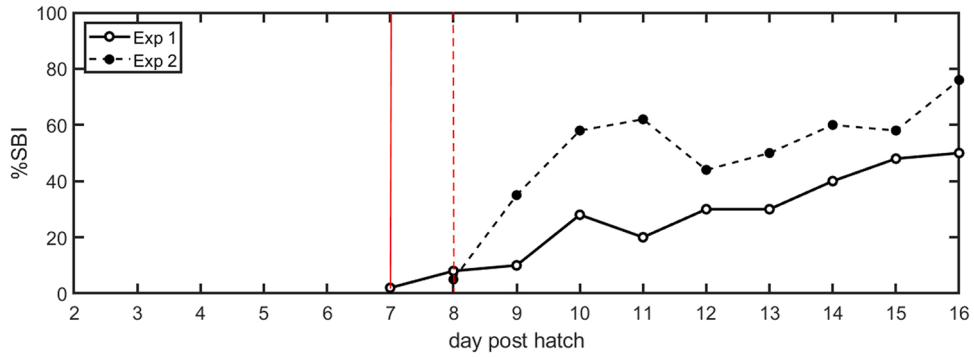

Fig. 6. Percentage of initial swimbladder inflation (% SBI) during the first days post-hatch for Exp 1 (solid line) and Exp 2 (dashed line). Vertical solid (Exp 1) and dotted (Exp 2) lines indicate the first detection of inflated swimbladders.

16-dph. The results show that the percentage increased throughout the experiment, reaching its maximum at the end of the experiment. We confirmed that between 16-dph and 17-dph this percentage did not change in our experience. The maximum percentage of inflated swimbladder in the larvae was 60% (L_s=5.4±0.6 mm) for Exp1 and 80% (L_s=5.7±0.6 mm) for Exp2.

3.2. Results from numerical simulations of the target strength of gilthead seabream

As mentioned above, the swimbladder is a gas-filled organ within the body cavity and it behaves acoustically like a gas bubble. By disturbing the swimbladder with the ultrasonic beam, it gives a natural oscillation frequency. Studies have shown that the resonance frequency increases with the depth of the fish (Feuillade and Nero, 1998; Kloser et al., 2002; Lo/vik and Hovem, 1979) and is greater for smaller fish. According to Simmonds and MacLennan (2005), in the case of fish larvae it could be as much as 40 kHz. To ensure that the measurements were far from the swimbladder's resonant frequency, we calculated the corresponding resonant frequency following Kloser et al. (2002). In our experiment, the maximum resonant frequency value was close to 100 kHz, which corresponded to 7-dph larvae in Exp1. Our working frequency, 200 kHz, lies on the geometric region where the backscattering is almost constant, so it was not necessary to consider the resonance of the swimbladder in our calculations.

The results from the numerical evaluation of TS for the gilthead seabream larvae are shown (Fig. 8). To evaluate the backscattered acoustic field from the larvae, the geometries corresponding to sampled individuals were considered. Good quality images were chosen to reconstruct the larvae's shape. To predict and interpret the experimental results, for each observation day a new geometry based on the direct images (Fig. 7a and b) observed by the microscope was developed (Fig. 7c). The modelling process, meshing and the calculated backscattered acoustic field are illustrated in Fig. 7c and d.

The FEM model was performed on each reconstructed geometry, hence obtaining a daily TS numerical estimation. Fig. 8 shows the numerical TS value's evolution over time. It should be noted that there was a qualitatively higher increment in TS at 7-dph and 8-dph, related to the detection of inflated swimbladders. Similar behaviour was observed for the geometries corresponding to both experiments.

3.3. Results of measured target strength with individual traces

A study of individual traces was made in the period of control measurements (without aeration) for Experiment 1. They were analysed from 6-dph, when the inflation of the swimbladder has not yet begun, to 16-dph. No traces were detected in the previous days. Table 3 shows values of the mean TS, the number of traces detected (n), the percentage of larvae with a swimbladder (% SBI) observed and the size of the average standard length (Ls) measured each day. Mean TS from individual traces were compared with the numerical TS predictions (see Fig. 9).

An increase in the TS of the larvae over time was observed, due to the increase in the size of the larvae as well as to an increase in their swimbladder size and inflation rate. An increase can be seen not only in TS, but also in the number of traces detected from 7 to 8-dph, corresponding to the observation of inflated swimbladders in the samplings. It should be noted that this behaviour (higher TS values) was also found in the numerical predictions shown in the previous section.

Finally, from the data obtained in the traces, adjustments were made

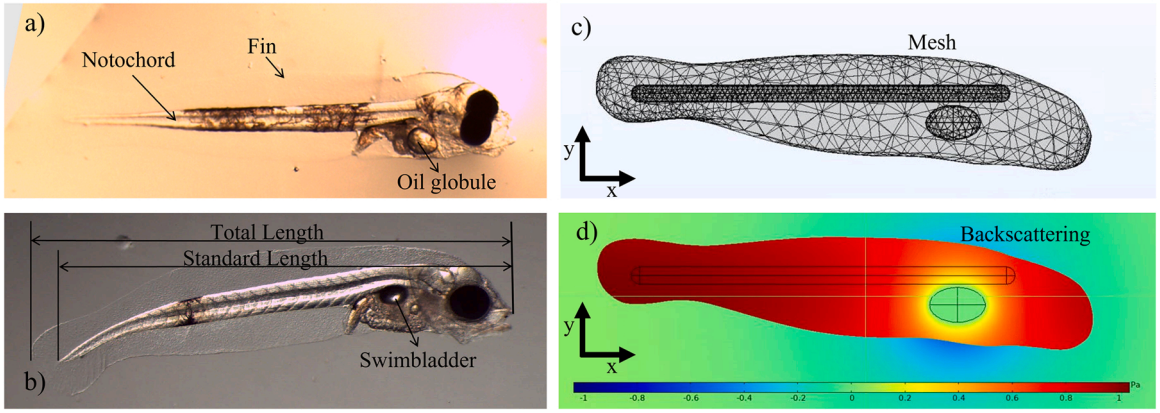

Fig. 7. Illustrative sketch of the geometry problem: (a) Generic representation of a larva at 5-dph (Exp1) with the oil globule. (b) Larva at 17-dph (Exp1) with a swimbladder. (c) Example of mesh discretisation used in the numerical calculations, with the internal surfaces (fin, notochord and swimbladder). (d) FEM simulation of acoustic backscattering of the larva with swimbladder.

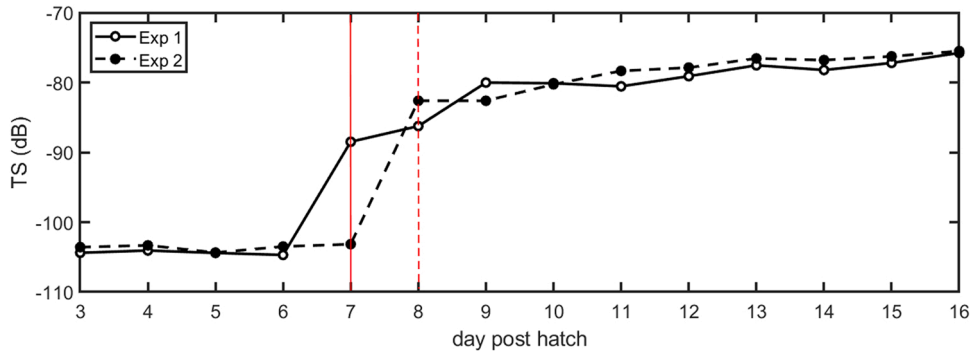

Fig. 8. Mean TS calculated at 200 kHz in FEM during the first days post-hatch of gilthead seabream larvae. The calculations were performed on geometries reproducing the observed samples. The vertical solid (Exp1) and dotted (Exp2) lines indicate the first detection of inflated swimbladders.

Table 3
Mean TS, number of traces (n), percentage of swimbladder inflated (%SBI) and the median standard length (*Ls*) values obtained from the analysis of unit traces of larvae between 6-dph and 16-dph (Exp1).

Day (dph)	Exp1			
	mean TS	n	% SBI	*Ls* (mm)
6	-85.6	8	0	3.75±0.19
7	-83.5	9	2	3.85±0.19
8	-82.3	111	8	3.9±0.2
9	-81.5	157	10	4.1±0.3
10	-80.8	160	28	4.2±0.3
11	-80.3	103	20	4.3±0.4
12	-77.8	392	30	4.5±0.5
13	-76.8	517	30	4.8±0.6
14	-76.6	93	40	5.0±0.6
15	-75.5	173	48	5.1±0.6
16	-74.9	176	50	5.7±0.6

between the TS and the standard length and between the TS and the swimbladder inflation rate, obtaining good correlation coefficients for both cases, as shown in Table 4.

3.4. Comparison between numerical simulations and target strength measurement under control conditions

The numerical simulations were compared with the experimental measurements under control conditions, when the aeration system was switched off. Numerical TS estimation can be directly compared with the TS values obtained for individual trace processing. Nevertheless, when the measurements were processed automatically, the median TS was calculated after applying an automatic SED algorithm. Unlike the individual trace processing, in this case there was no filter associated with the target behaviour. Single echoes were considered independently of their trajectory. In the automatic acoustic measurements, it should be considered that any target in the water column was insonified, contributing to the backscattered acoustic field. The presence of several targets simultaneously insonified, including larvae with and without a swimbladder, bubbles or food, generates multiple scattering with different amplitudes and resonance frequencies (Feuillade et al., 1996; Ye and Farmer, 1994). As consequence, background noise associated with multiple scattering is expected, giving rise to an increase in TS values, compared to individual trace results. For the sake of comparison, the value of background noise level was added to the numerical simulation. It was evaluated from the experimental mean TS value corresponding to the days before the first swimbladder inflation, with − 85.8 dB for Exp1 and − 81.6 dB for Exp2. The background noise level was not affected by any external parameter and corresponds only to the contribution from the larvae, food or the existence of minimal residual gas bubbles that dominate the backscattering. Fig. 9 shows good agreement between the numerical TS estimation and the experimental measurements under control conditions. Not only do the general trends agree with the values predicted from the numerical simulations, but even the median TS values from the individual traces, too.

For Exp1 data (Fig. 10a), the presence of an inflated swimbladder

Table 4
Parameters obtained from the linear regression adjustments of the logarithm of the standard length (*Ls*) versus mean TS, and of the percentage of swimbladders inflated (%SBI) versus mean TS for Exp 1.

	$TS(dB) = a \bullet log_{10}Ls(mm) + b$			
	a	b	r^2	p
Exp1	56.6	-116.1	0.91	< 0.01
	$TS(dB) = a \bullet (\%SBI) + b$			
	a	b	r^2	p
Exp1	0.19	-84.2	0.92	< 0.01

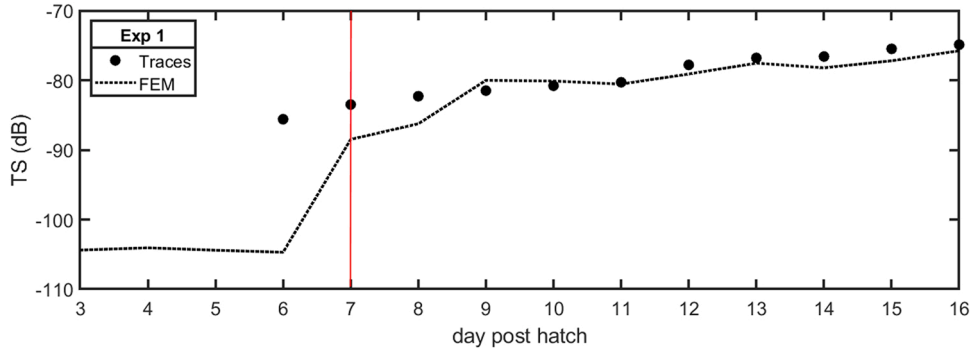

Fig. 9. Mean TS values of individual traces (circles) versus values of numerical simulations (dashed line) during the first days post-hatch for Exp 1. The vertical solid line indicates the first detection of inflated swimbladders.

was evidenced at 7-dph, with 2% of sampled larvae with a swimbladder. Under control conditions, at 7-dph, a TS of − 81.4 dB was recorded, whereas at 16-dph it came to − 74.8 dB (6.6 dB higher than at 7-dph). For Exp2 (Fig. 10b), the swimbladder inflation process was similar to Exp 1. At 8-dph, 5% of the sampled larvae had developed a swimbladder, with non-inflated swimbladders observed the previous days. Under control conditions, the median TS increased by 4.1 dB from 8-dph to 15-dph (from −72.6 dB up to −68.5 dB). From these data, it is shown that after swimbladder inflation, the larvae turned into powerful acoustic reflectors, increasing the total TS value inside the tank. Due to technical reasons, we could not obtain data under control conditions at 16-dph. Following the trend shown in Exp1, from 9-dph to the last day of the experiment, the TS values remained high.

3.5. Feasibility of swimbladder inflation detection under production conditions

With the aim of exploring the feasibility of the method without perturbing the usual larval rearing process, this section presents TS measurements under production conditions. This means that the aeration system was operational, and a lot of bubbles were present in the tank. As with the automatically processing of the acoustic data under control conditions, the median TS was calculated after applying an automatic SED algorithm. In the results for both experiments, it was observed that the control measurements generally have lower TS values than those measured under production conditions due to the higher background level introduced under production conditions, mainly by the presence of gas bubbles from the aeration system.

For Exp1, under production conditions, the median TS value was of − 76.3 dB. At 16-dph with 50% of larvae with a developed swimbladder, a TS value of − 70.5 dB was seen, meaning an increase of 5.8 dB compared to 7-dph (see Fig. 11a). For Exp2, the median TS increase was smaller: 2 dB, from − 70.5 dB at 8-dph up to − 68.5 dB at 16-dph (see Fig. 11b).

3.6. Acoustic monitoring of early gilthead seabream's larval growth

Finally, we wondered if the TS vs length relationship could be obtained on monitoring the larval growth during their early stages, once the first swimbladder inflation was detected. Linear regression adjustments between TS and $\log_{10}(L_s)$ were performed, (see Table 5). Firstly, we analysed the results obtained under production conditions (dashed line in Fig. 12). Secondly, we explored the results under control conditions (solid line in Fig. 12). Good correlations were obtained in both cases.

4. Discussion

As expected, the results from biological samplings agreed with previous publications. Swimbladder inflation was observed at around 8-dph (Kitajima et al., 1977) when the larvae's size was around 4.0 mm (Chatain, 1986) for both experiment replicates. From the time of the first inflation, the larvae's length grew more rapidly, as can be seen in Fig. 5a. The swimbladder inflation rate increased until reaching its maximum value around 15-dph or 16-dph, as had been previously reported (Chatain, 1986). These results are standard in rearing processes for *Sparus aurata*.

The working hypothesis was fundamentally that swimbladder inflation could be detected using non-invasive ultrasonic techniques. The results from the numerical TS estimations confirmed this (see Fig. 8), predicting a TS increase of around 20 dB when the swimbladder inflates due to the presence of gas. It should be remembered that the numerical model was developed using the sampling images in each case and not using simplified models, which, while useful for describing general trends and close numerical results, are not able to describe particular details for each experiment.

To confirm the numerical prediction, we performed acoustic measurements using a 200 kHz split-beam transducer (ES200-7C) operated by a Simrad EK60 echosounder. The manual detection of individual traces was compared with the numerical estimations for Exp1. The restrictions to the traces, processed by a trained operator, acted as a filter

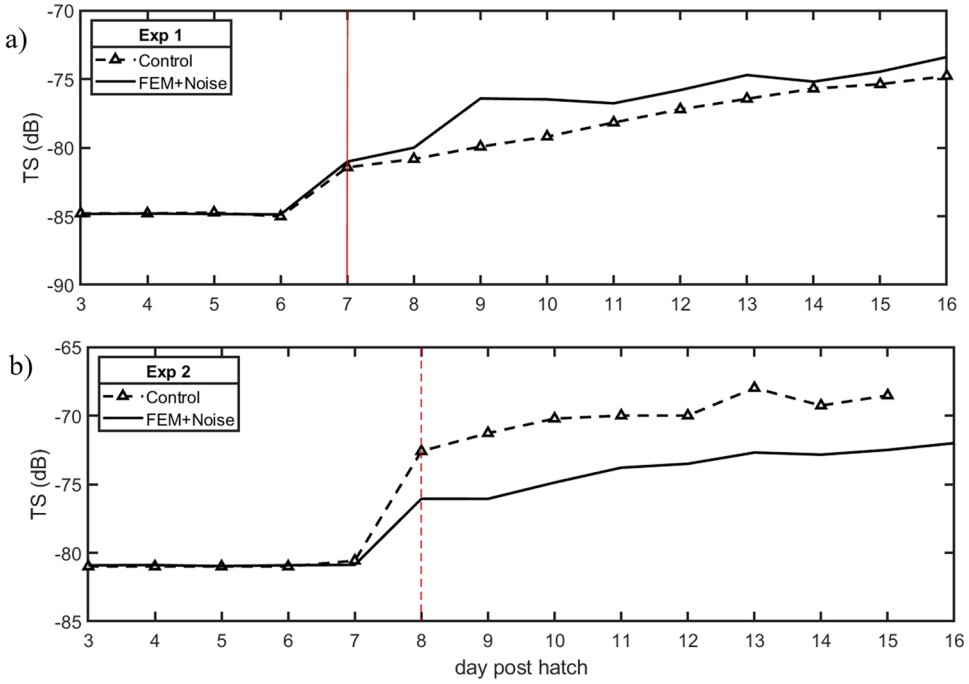

Fig. 10. Median TS values from experimental measurements under control conditions (triangles and dashed line) versus mean TS values from numerical simulations (solid line) for Exp1 (a) and Exp2 (b) during the first days post-hatch. The vertical solid (Exp1) and dotted (Exp2) lines indicates the first detection of inflated swimbladders.

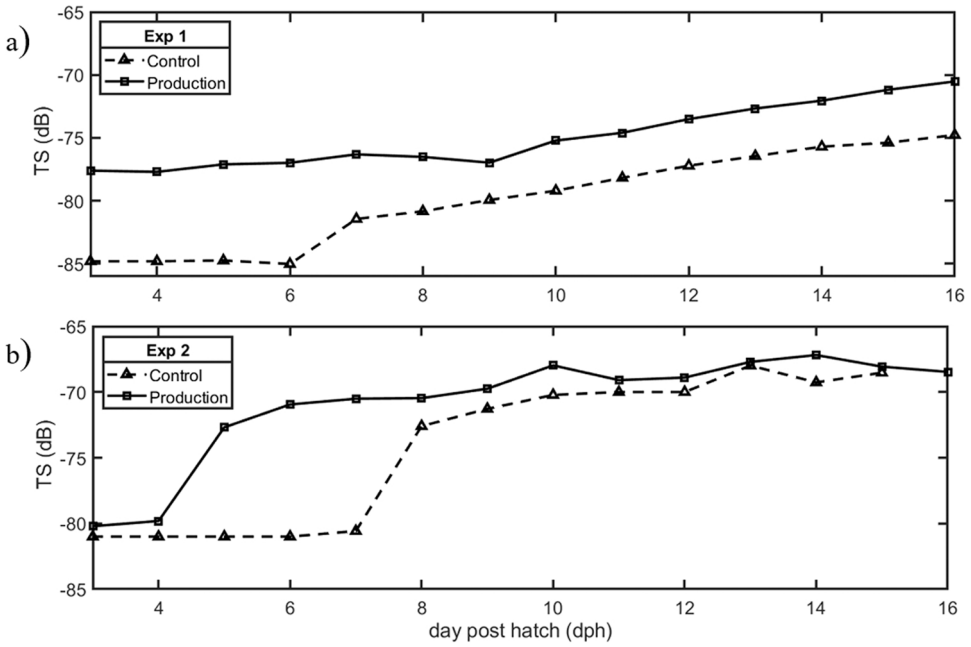

Fig. 11. Median TS values for night-time from 3-dph to 16-dph in Exp 1 (a) and in Exp 2 (b) obtained under control condition (triangles and dashed line) and under production condition (squares and solid line).

Table 5
Linear regression parameters for median TS versus logarithm of the standard length (*Ls*) for Exp 1 and Exp 2 under control and under production conditions.

Experiment		$TS(dB) = a \bullet log_{10}Ls(mm) + b$				
		a	b	r	r^2	p
Exp 1	Production	39.82	-99.96	0.97	0.94	< 0.01
	Control	40.81	-104.56	0.97	0.94	< 0.01
Exp 2	Production	16.41	-79.93	0.85	0.72	< 0.01
	Control	26.77	-88.24	0.95	0.91	< 0.01

to select the traces corresponding exclusively to larvae, and they can be directly compared to the numerical estimation. On one hand, a very good agreement is noticeable between the numerical predictions and the mean TS from individual traces (see Fig. 9). On the other hand, it is also noted that there were almost no traces detectable before the inflation of the swimbladder and the number of detections was significant only after the first inflation. This confirms that the method enables experimental monitoring of the swimbladder's inflation using echosounding techniques.

Once we had experimentally confirmed our main assumption, we

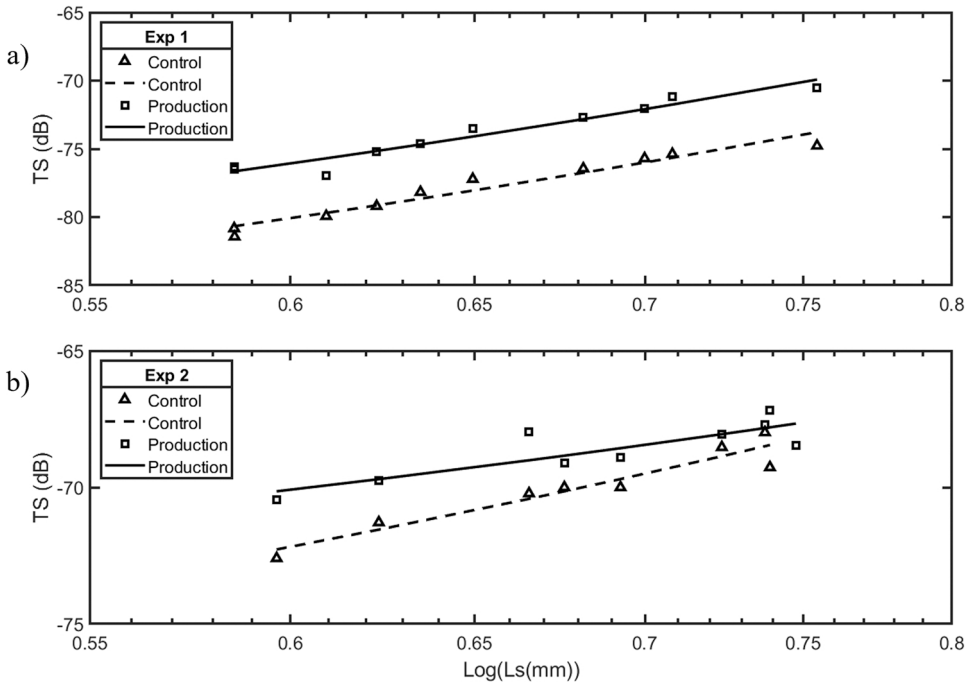

Fig. 12. Median TS values from the experimental under control condition (triangles) and under production condition (squares) measurements versus the logarithm of standard length (*Ls (mm)*) for Exp 1 (a) and Exp 2 (b) and corresponding linear adjustment: dashed line (control condition) and solid line (production condition).

wondered if the acoustic detection of inflation processing could be automated. Results for measurements under control conditions with an automatic SED algorithm had also shown good agreement with numerical predictions considering the background noise due to multiple scattering (see Fig. 10). Slight quantitative discrepancies can be noted for the results in Exp2 (Fig. 10), where the measured TS data were larger than the numerical estimation. This could be related to the presence of residual bubbles in the tank leading to an underestimation of the background noise value applied to the numerical results. Qualitative trends under control conditions were the same for both experiments. An almost constant mean TS value was observed before the first inflation, whereas it monotonically increased after the first inflation, from then on providing a tool for automatic non-invasive detection of the beginning of swimbladder inflation. Furthermore, with the aim of exploring the feasibility of the inflation detection method to be introduced into the usual larval rearing process, we analysed the acoustic measurements under production conditions. It should be remarked that inflation was also detected in a similar way as for the control conditions results for Exp1, but although similar trends were observed for Exp2, we recorded high mean TS levels before the swimbladder inflation occurred. This is related to the presence of bubbles in the tank large enough to be comparable to the swimbladder's size at the early development stages. To incorporate the method into the rearing procedure under production conditions, a previous adjustment of the aeration and a flow-through system will be needed to ensure that airflow does not vary, thereby allowing bubbles' size to be controlled throughout the system. The capacity for monitoring without perturbing the rearing procedure is even more relevant on being applied to species with difficult larval rearing (Dhert et al., 1998), and the technique presented could improve rearing management in such species.

As a last step, we considered the relationship between the mean TS and larvae's length, in a similar way as is done for fish (Love, 1971). When we explored the relationship between the mean TS from individual traces for Exp 1 and larvae length, a very good linear regression was obtained, given by $TS = 56.6L_s - 116.1$ (r^2=0.91). This confirmed that the mean TS could provide a tool for monitoring larval growth during early development. Looking deeper into the process for automating processing, we performed a similar regression adjustment for the mean TS measurements obtained using an automatic SED algorithm for both replicas, obtaining a very good linear correlation for both experiments. Moreover, good correlations between mean TS and larvae length were also obtained for measurements performed under production conditions. This could provide an additional technique to monitor early larval development to be introduced into the usual rearing procedure.

5. Conclusions and further work

Experimental analyses and numerical simulations of the backscattered acoustic intensity of seabream larvae up to 16 days post-hatch were carried out. Early larval growth, swimbladder area and inflation rate were monitored from 3-dph to the end of experiment. The numerical estimation of TS has been proven as a useful tool for predicting and interpreting acoustic backscattering of larvae even in the early stages of larval development. With respect to the acoustic TS measurements, the general trend can be described as follows: during the first post-hatching days it is almost constant, with a low TS value recorded, related to the scattering of residual bubbles, larval food and larvae without an inflated swimbladder. As of the first swimbladder inflation, the TS values then increase over time (Fig. 9 and Fig. 10). This enables acoustic detection of when the swimbladder inflation begins. From this moment, the inflation rate and swimbladder area on one hand and the early larval growth on the other can be monitored by measuring and processing the TS automatically, providing a non-invasive technique to monitor swimbladder inflation and larval growth. It should be remarked that this tool can be applied even under working conditions and therefore it does not interfere in the usual rearing process. Swimbladder inflation is related to larval morphological quality and survival rate for several fish species, so monitoring it could help improve the knowledge and efficiency of larval fish rearing (Doroshev et al., 1981). In this study, it has been tested on a particular species, *Sparus aurata*, but in future it could be extrapolated to other species and could be especially useful in improving the cultivation of more delicate species (Kurata et al., 2012). An additional development of automated systems for the control and characterization of aeration flow would be necessary to incorporate this technique to the actual rearing tanks.

CRediT authorship contribution statement

Anderson Ladino: Formal analysis, Methodology, Investigation, Data curation, Writing – original draft. **Vicente Puig Pons:** Software, Methodology, Investigation, Writing – original draft. **Victor Espinosa:** Conceptualization, Supervision, Project administration, Funding acquisition, Writing – review & editing. **Isabel Pérez-Arjona:** Conceptualization, Methodology, Validation, Writing – original draft, Writing – review & editing, Visualization. **Fernando de la Gándara:** Resources, Methodology, Supervision. **Aurelio Ortega:** Resources, Methodology, Supervision.

Declaration of Competing Interest

The authors declare that they have no known competing financial interests or personal relationships that could have appeared to influence the work reported in this paper.

Acknowledgements

This work was supported by funding from Generalitat Valenciana (Regional Valencia Government) through the AICO/2020/064 project and the Spanish Government through ACUSTUNA project ref. CTM2015-70446-R (MINECO/ERDF, EU), financing the experimental work carried out in the context of the competitive access ACUSTUNA in the ICTS-ICAR (www.icar.ieo.es). Funding for open access charge: CRUE−Universitat Politècnica de València. The authors want to thank UPV's former master students L. L. Carrillo and F. A. Muñoz for their collaboration in preliminary works.

References

Andrades, J.A., Becerra, J., Fernandez-Llebrez, P., 1996. Skeletal deformities in larval, juvenile and adult stages of cultured gilthead sea bream (Sparus aurata L.). Aquaculture 141 (1–2), 1–11. https://doi.org/10.1016/0044-8486(95)01226-5.

APROMAR, 2021. La acuicultura en España 2021. ⟨http://apromar.es/⟩ (Accessed 28 December 2021).

Berenger, J.P., 1996. Three-dimensional perfectly matched layer for the absorption of electromagnetic waves. J. Comput. Phys. 127 (2), 363–379. https://doi.org/10.1006/jcph.1996.0181.

Boglione, C., Gagliardi, F., Scardi, M., Cataudella, S., 2001. Skeletal descriptors and quality assessment in larvae and post-larvae of wild-caught and hatchery-reared gilthead sea bream (Sparus aurata L. 1758). Aquaculture 192 (1), 1–22. https://doi.org/10.1016/S0044-8486(00)00446-4.

Boyra, G., Moreno, G., Sobradillo, B., Pérez-Arjona, I., Sancristobal, I., Demer, D.A., 2018. Target strength of skipjack tuna (Katsuwanus pelamis) associated with fish aggregating devices (FADs). ICES J. Mar. Sci. 75 (5), 1790–1802. https://doi.org/10.1093/icesjms/fsy041.

Brewer, G., Kleppel, G., 1986. Diel vertical distribution of fish larvae their prey in nearshore waters of southern California. Mar. Ecol. Prog. Ser. 27 (1), 217–226. https://doi.org/10.3354/meps027217.

Ceballos-Francisco, D., Carrillo, N.G., Pardo-Fernández, F.J., Cuesta, A., Esteban, M., 2020. Radiological characterization of gilthead seabream (Sparus aurata) by X-ray computed tomography. J. Fish. Biol. 97 (5), 1440–1447. https://doi.org/10.1111/jfb.14510.

Chatain, B., 1986. The swimbladder in Dicentrarchus labrax and Sparus auratus. II. Influence of developmental anomalies on larval growth. Aquaculture 65, 175–181. https://doi.org/10.1016/0044-8486(86)90361-3.

Chatain, B., 1994. Abnormal swimbladder development and lordosis in sea bass (Dicentrarchus labrax) and sea bream (Sparus auratus). Aquaculture 119 (4), 371–379. https://doi.org/10.1016/0044-8486(94)90301-8.

Chatain, B., Ounais-Guschemann, N., 1990. Improved rate of initial swim bladder inflation in intensively reared Sparus auratus. Aquaculture 84 (3–4), 345–353. https://doi.org/10.1016/0044-8486(90)90099-9.

Chu, D., Wiebe, P.H., Copley, N.J., Lawson, G.L., Puvanendran, V., 2003. Material properties of North Atlantic cod eggs and early-stage larvae and their influence on acoustic scattering. ICES J. Mar. Sci. 60 (3), 508–515. https://doi.org/10.1016/S1054-3139(03)00047-X.

Comsol, 2021. Acoustics Module User's Guide, 2021. ⟨https://doc.comsol.com/6.0/doc server/#!/com.comsol.help.comsol/helpdesk/helpdesk.html⟩ (Accessed 28 December 2021).

Davis, T.L.O., Jenkins, G.P., Young, J.W., 1990. Patterns of horizontal distribution of the larvae of southern bluefin (Thunnus maccoyii) and other tuna in the Indian Ocean. J. Plankton Res. 12 (6), 1295–1314. https://doi.org/10.1093/plankt/12.6.1295.

Del Pilar Ruso, Y., Bayle-Sempere, J.T., 2006. Diel and vertical movements of preflexion fish larvae assemblages associated with Posidonia oceanica beds. Sci. Mar. 70 (3), 399–406. https://doi.org/10.3989/scimar.2006.70n3399.

Dhert, P.H., Divanach, P., Kentouri, M., Sorgeloos, P., 1998. Rearing techniques for difficult marine fish larvae. World Aquac. (1).

Doroshev, S.I., Cornacchia, J.W., Hogan, K., 1981. Initial swim bladder inflation in the larvae of physoclistous fishes and its importance for larval culture. Cons. Perm. Int. Pour l'Explor. De. la Mer. 178, 495–500.

Feuillade, C., Nero, R.W., 1998. A viscous-elastic swimbladder model for describing enhanced-frequency resonance scattering from fish. J. Acoust. Soc. Am. 103 (6), 3245–3255. https://doi.org/10.1121/1.423076.

Feuillade, C., Nero, R.W., Love, R.H., 1996. A low-frequency acoustic scattering model for small schools of fish. J. Acoust. Soc. Am. 99 (1), 196–208. https://doi.org/10.1121/1.414503.

Foote, K.G., 1980. Importance of the swimbladder in acoustic scattering by fish: a comparison of gadoid and mackerel target strengths. J. Acoust. Soc. Am. 67 (6), 2084–2089. https://doi.org/10.1121/1.384452.

Foote, K.G., 1987. Fish target strengths for use in echo integrator surveys. J. Acoust. Soc. Am. 82 (3), 981–987. https://doi.org/10.1121/1.395298.

Furusawa, M., 1988. Prolate spheroidal models for predicting general trends of fish target strength. J. Acoust. Soc. Jpn. (E) 9 (1), 13–24. https://doi.org/10.1250/ast.9.13.

Georgakopoulou, E., Katharios, P., Divanach, P., Koumoundouros, G., 2010. Effect of temperature on the development of skeletal deformities in Gilthead seabream (Sparus aurata Linnaeus, 1758). Aquaculture 308 (1–2), 13–19. https://doi.org/10.1016/j.aquaculture.2010.08.006.

Gorska, N., Korneliussen, R.J., Ona, E., 2007. Acoustic backscatter by schools of adult Atlantic mackerel. ICES J. Mar. Sci. 64 (6), 1145–1151. https://doi.org/10.1093/icesjms/fsm094.

Ihlenburg, F., 1998. Finite Element Analysis of Acoustic Scattering. Applied Mathematical Sciences. Springer, Berlin. https://doi.org/10.1007/b98828.

Ito, Y., Yasuma, H., Masuda, R., Minami, K., Matsukura, R., Morioka, S., Miyashita, K., 2011. Swimming angle and target strength of larval Japanese anchovy (Engraulis japonicus). Fish. Sci. 77 (2), 161–167. https://doi.org/10.1007/s12562-011-0323-1.

Jech, J.M., Horne, J.K., Chu, D., Demer, D.A., Francis, D.T.I., Gorska, N., Jones, B., Lavery, A.C., Stanton, T.K., Macaulay, G.J., Reeder, D.B., Sawada, K., 2015. Comparisons among ten models of acoustic backscattering used in aquatic ecosystem research. J. Acoust. Soc. Am. 138 (6), 3742–3764. https://doi.org/10.1121/1.4937607.

Kitajima, C., Iwamoto, H., Fujita, S., 1977. Relation between curvature of vertebral column and hatchery-reared undeveloped swimbladder in red sea bream, Pagrus major. Bull. Nagasaki. Pref. Inst. Fish. 3, 23–32.

Kitajima, C., Tsukamasa, Y., Fujita, S., Watanabe, T., Yone, Y., 1981. Relationship between uninflated swim bladders and lordotic deformity in hatchery-reared red sea bream Pagrus major. (in Japanese with English abstract). Bull. Jpn. Soc. Sci. Fish. 47, 1289–1294. https://doi.org/10.2331/suisan.47.1289.

Kitajima, C., Tsukashima, Y., Tanaka, M., 1985. The voluminal changes of swim bladder of larval Red Sea Bream Pagrus major. Bull. Jpn. Soc. Sci. Fish. 51 (5), 759–764. https://doi.org/10.2331/suisan.51.759.

Kloser, R.J., Ryan, T., Sakov, P., Williams, A., Koslow, J.A., 2002. Species identification in deep water using multiple acoustic frequencies. Can. J. Fish. Aquat. Sci. 59 (6), 1065–1077. https://doi.org/10.1139/f02-076.

Knudsen, F.R., Larsson, P., 2009. Discriminating the diel vertical migration of fish and Chaoborus flavicans larvae in a lake using a dual-frequency echo sounder. Aquat. Living Resour. 22 (3), 273–280. https://doi.org/10.1051/alr/2009029.

Knudsen, F.R., Larsson, P., Jakobsen, P.J., 2006. Acoustic scattering from a larval insect (Chaoborus flavicans) at six echosounder frequencies: implication for acoustic estimates of fish abundance. Fish. Res. 79 (1–2), 84–89. https://doi.org/10.1016/j.fishres.2005.11.024.

Kurata, M., Seoka, M., Nakagawa, Y., Ishibashi, Y., Kumai, H., Sawada, Y., 2012. Promotion of initial swimbladder inflation in Pacific bluefin tuna, Thunnus orientalis (Temminck and Schlegel), larvae. Aquac. Res. 43 (9), 1296–1305. https://doi.org/10.1111/j.1365-2109.2011.02933.x.

Langdon, S., Chandler-Wilde, S.N., 2007. Finite element methods for acoustic scattering. Notes of Department of Mathematics, 220. University of Reading, Whiteknights PO Box, Berkshire, UK.

Leis, J.M., 2004. Vertical distribution behaviour and its spatial variation in late-stage larvae of coral-reef fishes during the day. Mar. Freshw. Behav. Physiol. 37 (2), 65–88. https://doi.org/10.1080/10236240410001705761.

Li, D., Hao, Y., Duan, Y., 2020. Nonintrusive methods for biomass estimation in aquaculture with emphasis on fish: a review. Rev. Aquac. 12 (3), 1390–1411. https://doi.org/10.1111/raq.12388.

Lo/vik, A., Hovem, J.M., 1979. An experimental investigation of swimbladder resonance in fishes. Acoust. Soc. Am. 66 (3), 850–854. https://doi.org/10.1121/1.383238.

Love, R.H., 1971. Dorsal-aspect target strength of an individual fish. J. Acoust. Soc. Am. 49 (3B), 816–823. https://doi.org/10.1121/1.1912422.

Modica, A., Santulli, A., Curatolo, A., Cusenza, L., Palillo, L., D'amelio, V., 1993. Relationships between absence of functional swimbladder, calculosis and larval mortality in hatcheryreared gilthead sea bream, Sparus aurata L. Aquac. Res. 24 (4), 517–522. https://doi.org/10.1111/j.1365-2109.1993.tb00626.x.

Moretti, A., Pedini, M., Cittolin, G., Guidastri, R., 1999. Manual on Hatchery Production of Seabass and Gilthead Seabream, Volume 1. Food and Agriculture Organization of the United Nations, p. 1.

Murphy, H.M., Jenkins, G.P., Hamer, P.A., Swearer, S.E., 2011. Diel vertical migration related to foraging success in snapper Chrysophrys auratus larvae. Mar. Ecol. Prog. Ser., 433(Type II) 185–194. https://doi.org/10.3354/meps09179.

Neilson, J.D., Perry, R.I., 1990. Diel vertical migrations of juvenile fishes: an obligate or facultative process. Adv. Mar. Biol. 26, 115–168. https://doi.org/10.1016/S0065-2881(08)60200-X.

O'Driscoll, R.L., Macaulay, G.J., Gauthier, S., Pinkerton, M., Hanchet, S., 2011. Distribution, abundance and acoustic properties of Antarctic silverfish (Pleuragramma antarcticum) in the Ross Sea. Deep-Sea Res. Part II: Top. Stud. Oceanogr. 58 (1–2), 181–195. https://doi.org/10.1016/j.dsr2.2010.05.018.

Ona, E., 1990. Physiological factors causing natural variations in acoustic target strength of fish. J. Mar. Biol. Assoc. U.K. 70 (1), 107–127. https://doi.org/10.1017/S002531540003424X.

Pérez-Arjona, I., Godinho, L., Espinosa, V., 2020. Influence of fish backbone model geometrical features on the numerical target strength of swimbladdered fish. ICES J. Mar. Sci. 77 (7–8), 2870–2881. https://doi.org/10.1093/icesjms/fsaa160.

Pierce, A.D., 2019. Acoustics: An Introduction to its Physical Principles and Applications. Springer. https://doi.org/10.1007/978-3-030-11214-1.

Prestinicola, L., Boglione, C., Cataudella, S., 2014. Relationship between uninflated swim bladder and skeletal anomalies in reared gilthead seabream (Sparus aurata). Aquaculture 432, 462–469. https://doi.org/10.1016/J.AQUACULTURE.2014.06.020.

Shoji, J., Maehara, T., Tanaka, M., 1999. Diel vertical movement and feeding rhythm of Japanese Spanish mackerel larvae in the central seto inland sea. Fish. Sci. 65 (5), 726–730. https://doi.org/10.2331/fishsci.65.726.

Simmonds, J., MacLennan, D., 2005. Fisheries Acoustics. Theory and Practice. Blackwell Science, Oxford.

Simrad, E., 2008. Scientific echo sounder. Reference Manual. Release, 2, 16–48. ⟨https://epic.awi.de/id/eprint/29658/1/Sim2008a.pdf⟩. accessed 28 December 2021.

Sobradillo, B., Boyra, G., Pérez Arjona, I., Martnitez, U., Espinosa, V., 2021. Ex situ and in situ target strength measurements of European anchovy in the Bay of Biscay. ICES J. Mar. Sci. https://doi.org/10.1093/icesjms/fsaa242.

Tsaklis, P.V., 2010. Presentation of acoustic waves propagation and their effects through human body tissues. Hum. Mov. 11 (1), 58–65. https://doi.org/10.2478/v10038-009-0025-z.

Vizcaíno, A.J., Saéz, M.I., López, G., Arizcun, M., Abellán, E., Martínez, T.F., Cerón-García, M.C., Alarcón, F.J., 2016. Tetraselmis suecia and Tisochrysis lutea meal as dietary ingredients for gilthead sea bream (Sparus aurata L.) fry. J. Appl. Phycol. 28 (5), 2843–2855. https://doi.org/10.1007/s10811-016-0845-0.

Woolley, L.D., Qin, J.G., 2010. Swimbladder inflation and its implication to the culture of marine finfish larvae. Rev. Aquac. 2 (4), 181–190. https://doi.org/10.1111/j.1753-5131.2010.01035.x.

Ye, Z., Farmer, D.M., 1994. Acoustic scattering from swim-bladder fish at low frequencies. J. Acoust. Soc. Am. 96 (2), 951–956. https://doi.org/10.1121/1.410269.

Zampolli, M., Tesei, A., Jensen, F.B., Malm, N., Blottman, J.B., 2007. A computationally efficient finite element model with perfectly matched layers applied to scattering from axially symmetric objects. J. Acoust. Soc. Am. 122 (3), 1472–1485. https://doi.org/10.1121/1.2764471.